

## Effect of Ultrasonic and Mechanical Vibration on the Corrosion Behavior of Mg-3Zn-0.8Ca Biodegradable Alloy

S.M. Abd El Hallem<sup>1</sup>, I. Ghayad<sup>2,\*</sup>, M. Eisaa<sup>2</sup>, N. Nassif<sup>2</sup>, M.A. Shoeib<sup>2</sup>, H. Soliman<sup>2,\*</sup>

<sup>1</sup>Chemistry Department, Faculty of Science, Zagazig University, Zagazig, Egypt

<sup>2</sup>Central Metallurgical Research and Development Institute, CMRDI, P.O. Box: 87, Helwan, Cairo, Egypt

\*E-mail: [ighayad@yahoo.com](mailto:ighayad@yahoo.com)

Received: 20 September 2013 / Accepted: 5 January 2014 / Published: 2 February 2014

---

Magnesium alloys have got extensive attention as implant materials due to their biodegradability in the physiological environment and matching elastic modulus with natural bone. However, their poor corrosion resistance is a dominant problem that limits their clinical application due to the inhomogeneous distribution of the second phase. This paper investigated the effect of ultrasonic vibration (UV) and mechanical vibration (MV) treatment of Mg-3Zn-0.8Ca biodegradable alloy on its corrosion behavior in comparison to the as-cast alloy (CC). Corrosion tests indicated that the UV-treated specimen exhibited uniform corrosion resulting from the uniform compact fine grains with higher concentration of oxides. The corrosion resistance was found in the following order: UV alloy specimen > MV alloy specimen > As-cast alloy specimen. The potentiodynamic polarization experiments showed that the corrosion potential of the UV-treated and MV-treated alloy specimen shift in the noble direction compared with the as-cast alloy. Electrochemical impedance spectroscopy confirmed the same sequence of corrosion resistance.

---

**Keywords:** Corrosion; implants; ultrasonic vibration (UV); mechanical vibration (MV) ; as-cast (CC)

### 1. INTRODUCTION

Magnesium alloys would dissolve readily in aqueous solution containing chloride ions [1, 2]. This characteristic has recently inspired the biomaterial researchers to develop them as a new kind of biodegradable material [3-9]. However; the main disadvantage of the Mg-based alloys as implant materials is their poor corrosion resistance which is harmful to their clinical applications [10]. The mechanical integrity of as-cast and conventional extrusion magnesium alloys is often rapidly destroyed

after implantation before the healing of tissue due to the heavily pitting corrosion at grain boundaries in the physiological environment [11].

An appropriate alloying composition can improve the corrosion resistance, mechanical properties and the ease of manufacture of Mg-based materials. Ca or Zn is one of the most abundant nutritionally essential elements in the human body and has basic safety for biomedical applications. Zn helps to overcome the harmful corrosion effect of iron (Fe) and nickel (Ni) impurities that might be present in Mg alloys. Ca reduces oxidation in the molten condition and during heat treatment, it also improves the rollability. Mg–1Zn produced less hydrogen than many other binary Mg alloys in simulated body fluid (SBF). Ca & Zn act as grain refining agent which improves both corrosion resistance and mechanical properties. Ca ion concentration up to 50 mg/l, Zn ion concentration up to 60 mg/l, Mg ion concentration up to 1000 mg/l did not cause cell toxicity [12-14].

In order to improve the mechanical properties of magnesium, significant efforts have been taken to develop magnesium matrix composites (MMCs) because of their low density and superior specific properties including strength, stiffness and creep resistance [15]. To fabricate MMCs, micron size ceramic particles were widely used. Compared with the unreinforced magnesium alloys, the micro particles reinforced MMCs usually have a considerably improved strength, but also a significantly reduced ductility, which limits their widespread application. Stirring casting that utilizes mechanical stirring is a mostly used technique of producing MMCs that are reinforced by micro ceramic particles. A combination of good distribution and dispersion of micro particles can be achieved by stirring casting. However, it is extremely challenging for the conventional stirring casting to distribute and disperse nanoparticles uniformly in metal melts because of their large surface-to-volume ratio and their low wettability in metal melts.

Ultrasonic treatment is a simple and effective physical means for solidification control. In 1878, the ultrasonic vibration was firstly introduced into metallurgical application to refine grains [16]. When ultrasonic vibrations are coupled to the solidifying melts, microstructural changes occur including grain refinement, increased homogeneity and reduced segregation. Many studies on ultrasonic vibration are mainly focused on the as-cast grain refinement of low-melting alloys [17,18].

In the present work, 3.0 wt% Zn and 0.8 wt% Ca were chosen as alloying elements to Mg, aiming at improving the corrosion resistance of magnesium alloy. An ultra-fine grained Mg–Zn–Ca alloy with MgO phases precipitating in the grain interiors and clean grain boundaries has been prepared by mechanical vibration and ultrasonic vibration treatment. In order to clearly understand the corrosion behavior of the mechanical vibration and ultrasonic vibration treated Mg–Zn–Ca alloy, the as-cast samples were also studied as reference.

## 2. EXPERIMENTAL

### 2.1. Materials

The alloy with a chemical composition of Mg- 3 wt.% Zn- 0.8 wt%. Ca was prepared from pure Mg (99.99%), zinc (99.98%) and Ca (99.98%) using a laboratory resistance furnace. Zn and Ca were selected as alloying elements because they are essential elements to human body and through optimizing the contents of Zn and Ca, corrosion resistance of the alloy may be improved. The melt was

transferred to a semi-continuous casting machine at 650°C, about 50°C higher than the liquidus. After casting, one of the three fields which include low frequency electromagnetic field, power ultrasonic field and the compound field (combination of low frequency electromagnetic field and power ultrasonic field) was applied. To evaluate the different influences of the three fields, all conventional parameters were held constant to minimize oxidation during casting. The ultrasonic system consists of an ultrasonic generator with a maximum power output of 2 kW and a transducer with a fixed frequency of 20 kHz.

## 2.2. Testing methods

### 2.2.2. Electrochemical measurements

Electrochemical tests were carried out using Autolab Potentiostat/ Galvanostat (PGSTAT 30) in simulated body fluid (SBF). Before the corrosion tests, all samples were firstly ground with SiC papers progressively to 800 grits followed by ultrasonically cleaning in ethanol for 5 min. SBF is composed of [19] 8.8 g/l NaCl, 0.4 g/l KCl, 0.14 g/l CaCl<sub>2</sub>, 0.35g/ l NaHCO<sub>3</sub>, 1.0 g/l C<sub>6</sub>H<sub>6</sub>O<sub>6</sub> (glucose), 0.2 g/l MgSO<sub>4</sub> 7H<sub>2</sub>O, 0.1 g/l KH<sub>2</sub>PO<sub>4</sub> H<sub>2</sub>O, 0.06 g/l Na<sub>2</sub>HPO<sub>4</sub> 7H<sub>2</sub>O, pH 7.4, at a temperature 37°C. A three-electrode cell was used for the electrochemical testing. Testing specimen was used as the working electrode; a platinum rod as the auxiliary electrode and a saturated calomel electrode as the reference electrode. Potentiodynamic polarization curves were measured in the range -0.4 to 1 V with respect to E<sub>corr</sub> at a scan rate of 5 mVs<sup>-1</sup> and 37°C. The area of the working electrode exposed to the solution was 0.196 cm<sup>2</sup>. Polarization resistance of test specimens was measured using Linear Polarization technique where the specimen potential was scanned from -25 mV below the E<sub>corr</sub> up to 25 mV above the E<sub>corr</sub> using a scan rate of 0.2 mV/s. The slope of the obtained straight line gives the polarization resistance (R<sub>p</sub>). Electrochemical impedance spectroscopy (EIS) measurements were performed using scan frequency ranged from 60 kHz to 10 mHz, and the perturbation amplitude was 5 mV. In the immersion tests, each prepared sample was placed in a glass cell containing 200 ml SBF solution kept at 37°C for a week.

### 2.2.3. Surface characterization techniques

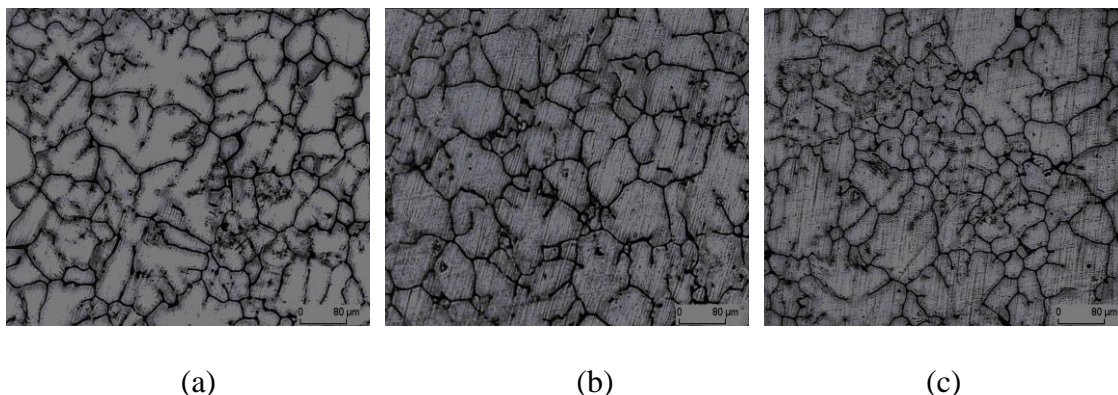
Microstructure and grain size of the tested alloy were investigated using optical microscope (Axiovision SE64 Rel.4.9). Surface morphology of tested specimens before and after corrosion tests was carried out using scanning electron microscope (SEM) JEOL, JSM 5410, Japan. Surface analysis was performed using energy dispersive spectroscopy unit attached to the SEM.

## 3. RESULTS AND DISCUSSION

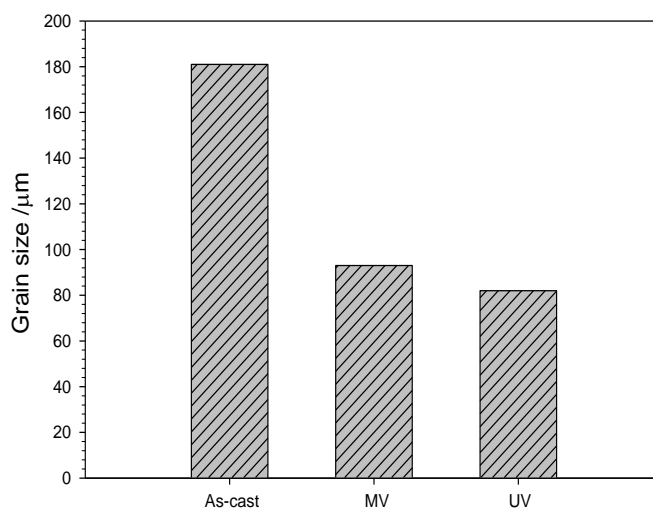
### 3.1. Microstructure investigation

Fig. 1 displays the optical micrographs of the as-cast, ultrasonically vibrated and mechanically vibrated alloy. The as-cast alloy shows coarse rosette grains. The vibrations wherever mechanical or

ultrasonic modify the structure to finely globular one. Fig. 2 presents the grain size of the alloy obtained by ultrasonic vibration, mechanical vibration and as- cast alloy. It can be seen that the grain size decreases in the order: as cast mechanical > ultrasonic. Average grain sizes of about 191, 93 and 82  $\mu\text{m}$  were obtained for the as-cast, MV and UV specimens, respectively. The highest extent of grain refinement is exhibited by the ultrasonically vibrated specimen.



**Figure 1.** Microstructure of the as-cast (a), mechanically vibrated (b) and ultrasonically vibrated (c) specimens, X= 100



**Figure 2.** Grain size of Mg-Ca-Zn alloys

### 3.2. Electrochemical Corrosion Tests

Fig. 3 shows the potentiodynamic polarization curves of the alloy specimens prepared by mechanical vibration, ultrasonic vibration as well as the as-cast alloy. The corrosion potential ( $E_{\text{corr}}$ ) shifts towards more anodic values in the order: ultrasonic vibration > mechanical vibration > as-cast alloy, pointing to a clear delay of the corroding phenomena. Potentiodynamic curves show very narrow passive region of about 200 mV followed by a rapid increase in current till it reaches a steady value of

about  $0.003 \text{ A cm}^{-2}$ . The relation between the potential and the recorded current density in the Tafel region (250 mV below and above  $E_{\text{corr}}$ ) is defined by the Tafel equation [20]:

Tafel equation for the anodic reaction  $\eta = \text{Log}(i_{\text{corr}}) + \beta_a \text{Log } i \quad (1)$

Tafel equation for the cathodic reaction  $\eta = \text{Log}(i_{\text{corr}}) - \beta_c \text{Log } i \quad (2)$

Where  $\eta$  is the overpotential;  $i$  is the current density;  $\beta_a$  and  $\beta_c$  are the Tafel constants characteristic of the electrode system. A plot of electrode potential against the logarithm of the current density is called the "Tafel plot" and the resulting straight line the "Tafel line". From the Tafel plot, the corrosion current is measured at the intersection of tangents drawn for the anodic and cathodic branches of the polarization curves.  $i_{\text{cor}}$  values of  $9.38 \times 10^{-7}$ ,  $9.24 \times 10^{-7}$  and  $7.54 \times 10^{-7} \text{ A cm}^{-2}$  were obtained for the as-cast, mechanically vibrated and ultrasonically vibrated, respectively.

The polarization resistance ( $R_p$ ) determined using linear polarization technique is shown in Fig.4.  $R_p$  increases in the following order: as-cast < mechanically vibrated < ultrasonically vibrated which means that the ultrasonically vibrated specimen gives the highest corrosion resistance followed by the mechanically vibrated specimen while the as-cast specimen gives the lowest corrosion resistance.

Fig.5 presents Nyquist plots of the as-cast, mechanically vibrated and ultrasonically vibrated alloy specimens. Nyquist plots show that the charge transfer resistance ( $R_{ct}$ ) as indicated by the diameter of the capacitance loop increases in ultrasonically vibrated alloy followed by the mechanically vibrated alloy and then the as-cast alloy. These results confirm the results of potentiodynamic experiments that ultrasonically and mechanically treated specimens have high corrosion resistance compared to the as-cast alloy.

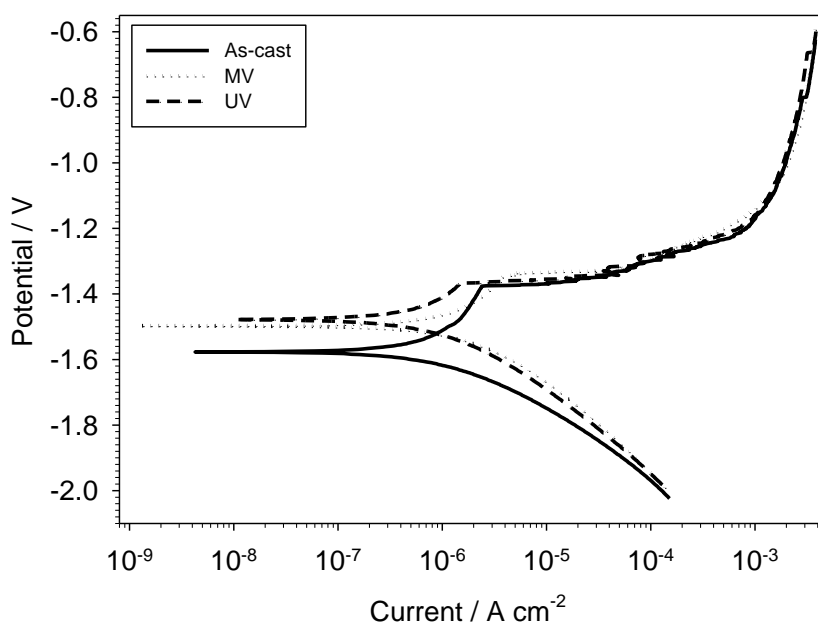


**Figure 3.** Potentiodynamic polarization curves of as-Cast, Ultrasonically vibrated and mechanically vibrated Mg-0.8Ca-3Zn in SBF solution at 25°C and 5 mV/s scan rate.

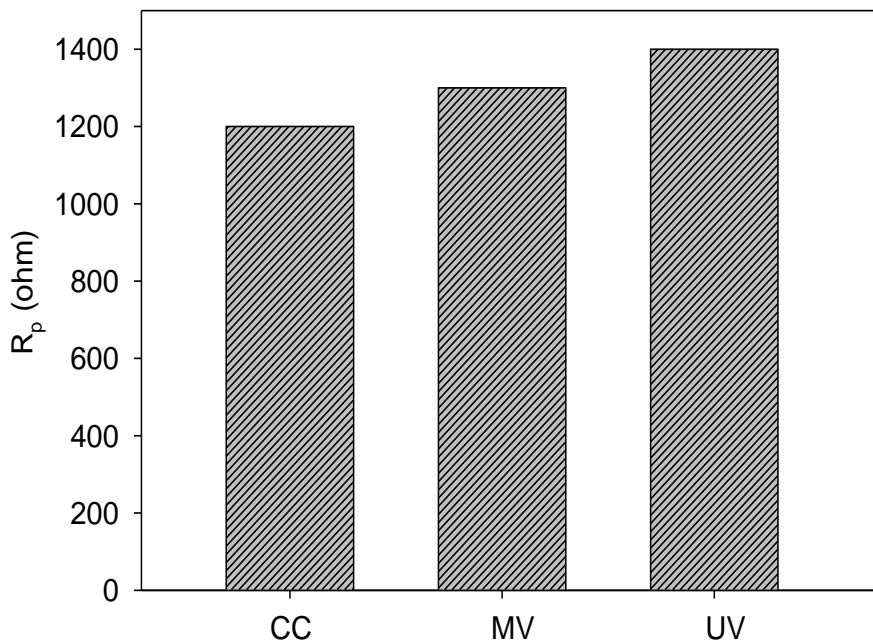


**Figure 4.** Polarization resistance of as-Cast, ultrasonically vibrated and mechanically vibrated Mg-0.8Ca-3Zn determined by linear polarization technique.

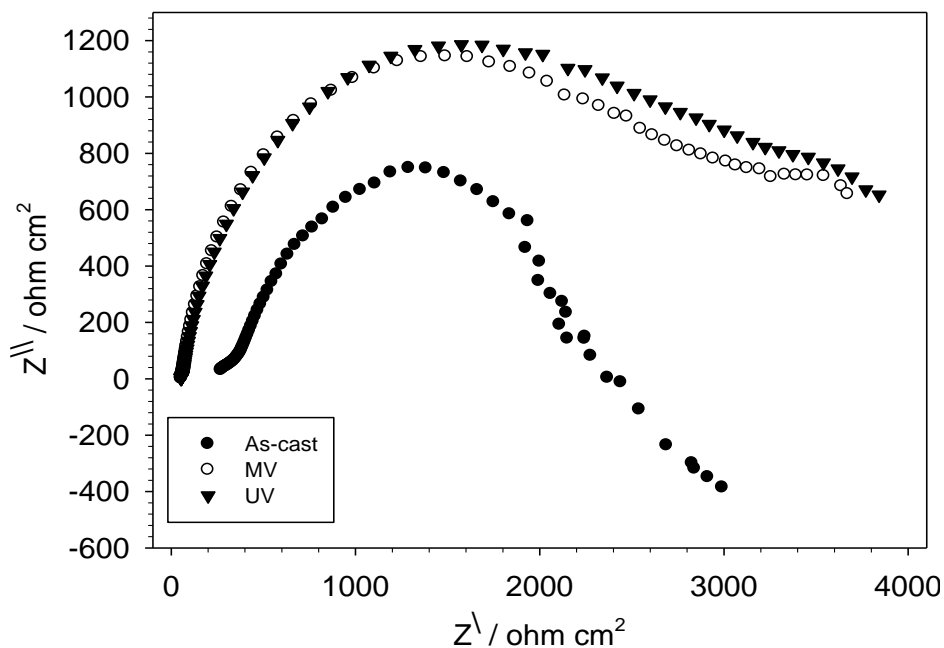


**Figure 5.** Nyquist plots of as-Cast, ultrasonically vibrated and mechanically vibrated Mg-0.8Ca-3Zn in SBF solution at 25°C.

Fig.6 represents the EIS pattern of investigated alloy specimens after immersion in the SBF solution at 37°C for different time intervals (1-7 days). Specimen having dimensions of 15 mm × 15 mm × 2mm were used for this test.

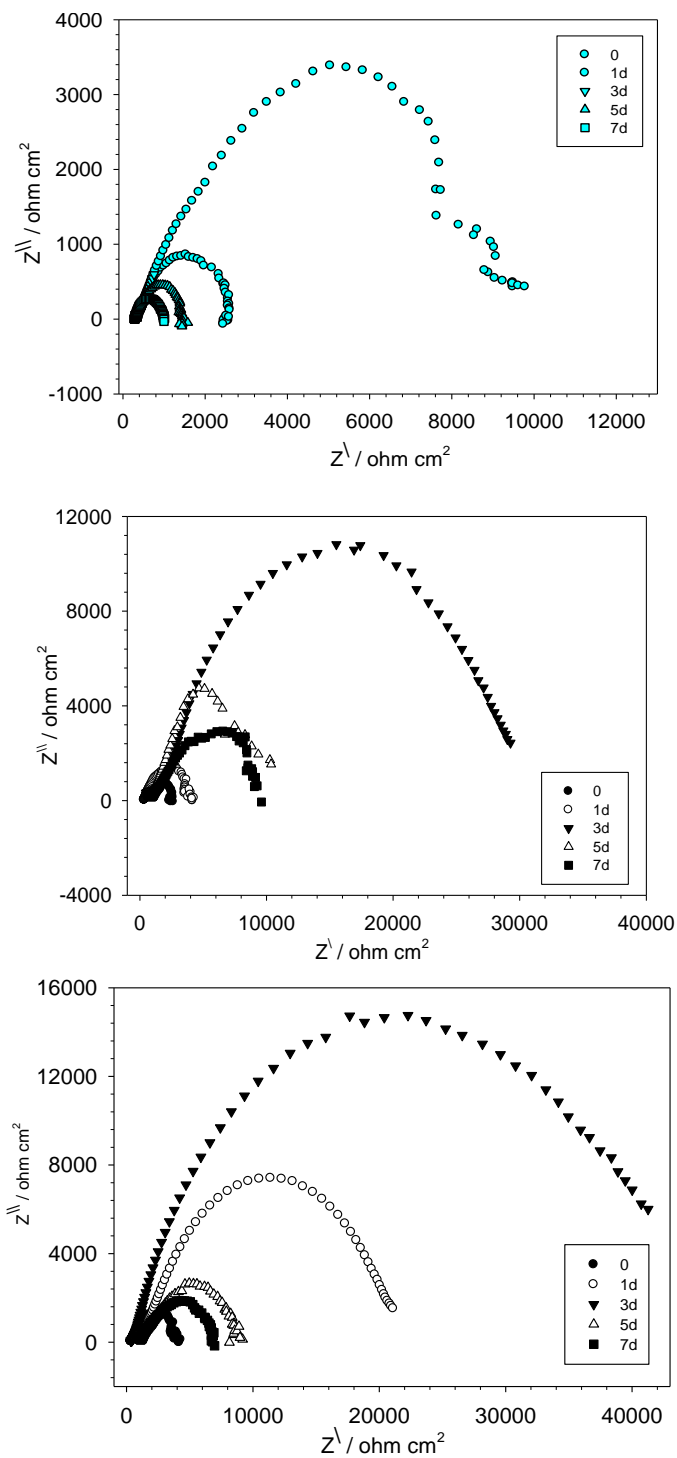


**Figure 6.** EIS pattern of specimens immersed 1-7 days in SBF at 37°C; (a) as-cast alloy, (b) mechanical vibration alloy and (c) ultrasonic alloy.

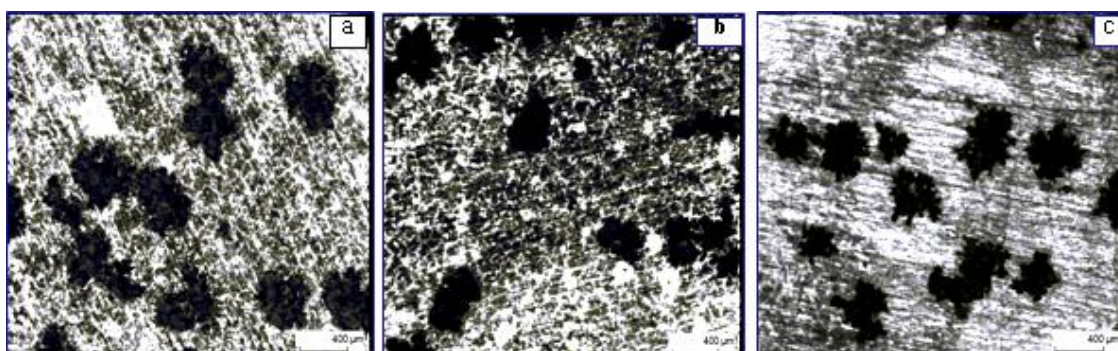
For the as cast alloy specimen, the protective layer reach its maximum resistance after 1day then begins to decrease. Ultrasonically and mechanically treated alloy specimens give the optimum resistance after 3 days then starts to decrease. It could be clearly seen that the degree of corrosion damage was much lower for ultrasonically and mechanically treated specimens. In addition, more

sever corrosion was observed for the as-cast alloy which is consistent with the electrochemical measurements.

### 3.3. Surface characterization of corroded samples

#### 3.3.1. Optical Microscopic investigation

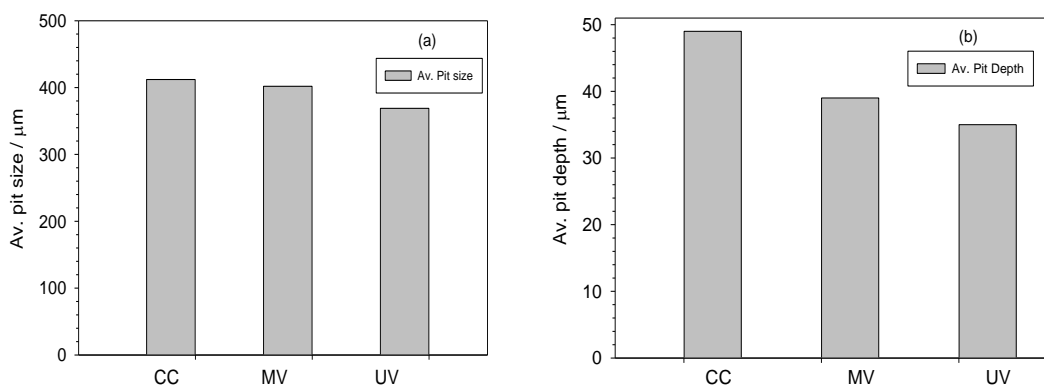
Fig.7 shows the optical microscopic photographs of as-cast, MV and UV specimens surfaces after potentiodynamic corrosion testing. The MV and UV specimens reveal small size pits with more corrosion resistant surface. Contrarily the as-cast alloy exhibits large deepest pits with deteriorated surface. It is clear that grain refining increases noticeably the corrosion resistance of MV and UV alloy.



**Figure 7.** Optical images for as –cast (a) , mechanically vibrated (b) and ultrasonically vibrated (c) specimens after potentiodynamic polarization test.

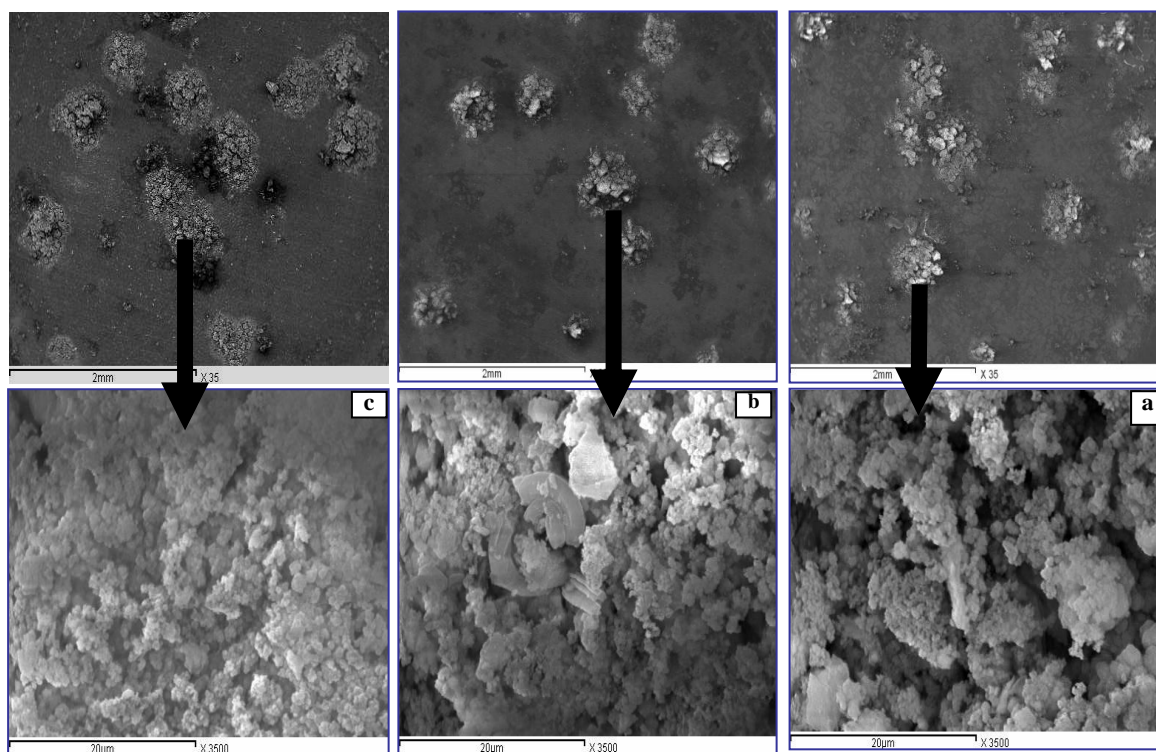
The effect is more pronounced in specimens prepared by the UV method [21,22]. When the microstructure is some what coarse as in the case of as-cast alloy specimen, the corrosion protection becomes weak as shown by the as-cast alloy.

The average size and depth of pits as determined under the optical microscope is shown in Fig.8. The pit depth is determined by focusing on the surface of a pit and subtracting the reading of the fine focusing knob from the knob reading upon focusing on the bottom of the pit. Both size and pit depth is decreases in the order: ultrasonic vibration < mechanical vibration < as-cast alloy



**Figure 8.** Average pit size (a) and depth (b) of CC , MV and UV Mg-3Zn-0.8Ca alloy after potentiodynamic polarization testing in SBF.

### 3.3.2. Scanning Electron Microscopic (SEM) Investigation



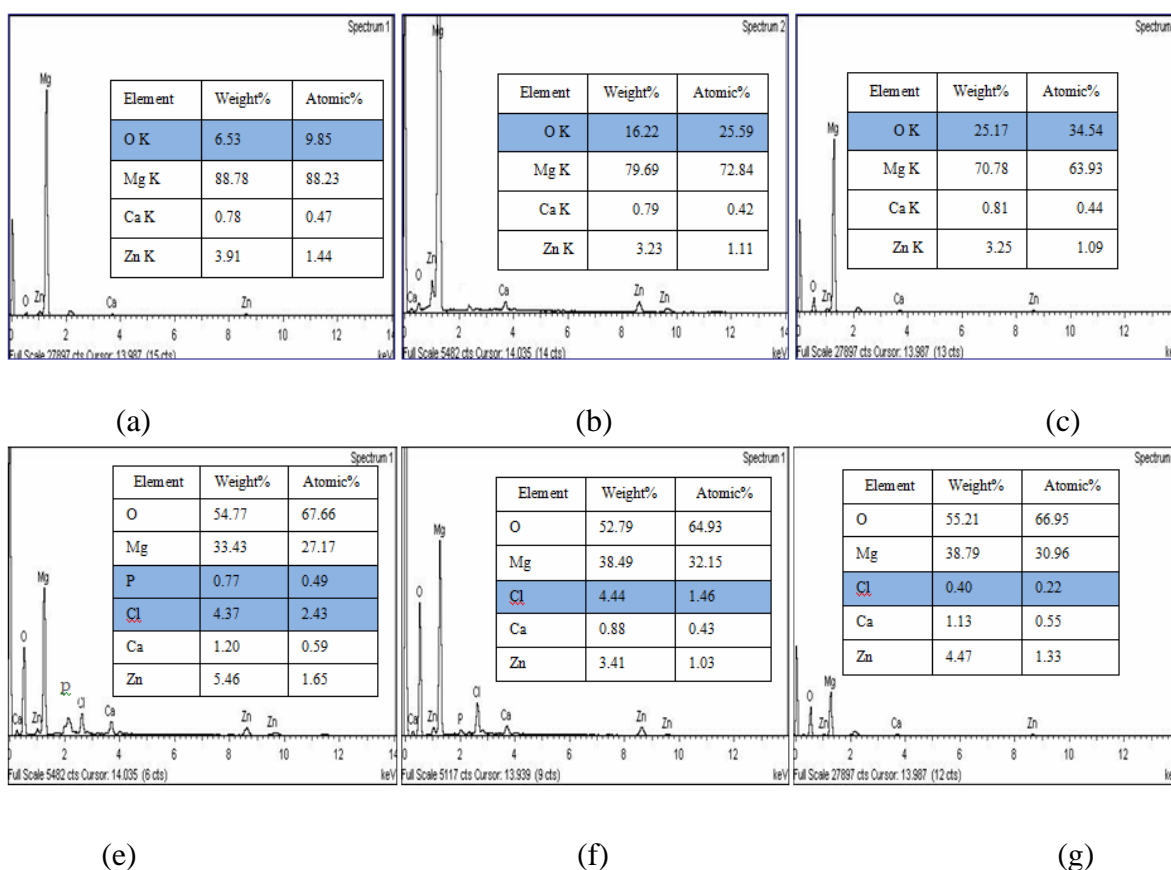
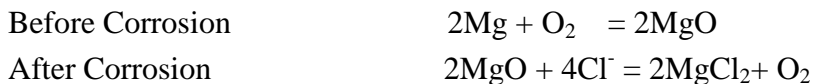
**Figure 9.** SEM images for (a) ultrasonic vibration (b) mechanical vibration (c) as –cast after potentiodynamic polarization testing in SBF.

Fig.9 represents the surface morphology investigated by the scanning electron microscope (SEM) of tested specimens after potentiodynamic polarization tests. The corrosion attack is more obvious on the surface of the as-cast alloy specimen surface followed by the MV specimen while the UV specimen shows the least corrosion attack. Corrosion attack manifests itself by rougher surface and higher degree of porosity. It is suggested that the corrosion products acts as a barrier between the specimen surface and the corrosive solution. In case of the as cast-alloy, the highly porous layer does not well protect the alloy surface against corrosion and allows fast reaction between the alloy and the SBF solution causing rapid generation of hydrogen gas bubbles on the alloy surface [21]. So, the black spots appear on surface of the as-cast alloy reveal due to corrosion holes formed during degradation of the alloy. Thus, ultrasonic and mechanical vibration markedly enhances corrosion resistance than as-cast alloy that coincide with previous results.

### 3.3.3. Energy Dispersive X-Ray Spectroscopy Investigation

Fig.10 confirms the chemical composition of the alloy (Mg-3% Zn-0.8% Ca). EDX surface analysis showed also different contents of oxygen (oxides). The existence of oxygen in the protective film is due to hydroxides of Mg ( $\text{Mg}(\text{OH})_2$ ). These corrosion products act as barrier films to protect the surface from aggressive solution [23]. UV alloy specimen shows the highest content of O as result of finer grains.

After corrosion test, the EDX analysis of the as-cast alloy indicates the presence of magnesium, calcium, phosphorus, oxygen, and carbon elements which implied the formation of hydroxyapatite (HA). Meanwhile, the Ca/P ratio is 1.6 that is related to hydroxyapatite formation. The UV alloy sample contains the least amount of chloride content while the as-cast alloy specimen contains the highest amount of chloride content. Chloride ions are small enough to displace water molecules in the hydrogen sheath and then preferentially combines with  $Mg^{2+}$  to transform magnesium hydroxide into soluble  $MgCl_2$ . Therefore, the variations of the OCP values could be attributed to the dissolution–precipitation process of  $Mg(OH)_2$  film layer in the SBF solution [20,21].



**Figure 10.** EDX analysis of (a) as –cast (b) MV (c) UV before corrosion testing and (e) as-cast (f) MV (g) UV after corrosion testing.

**4. CONCLUSIONS**

On the basis of the present studies, the following conclusions may be drawn:

- 1) Ultrasonic and mechanical vibration treatment obviously modified the microstructure of Mg-3Zn-0.8Ca biodegradable alloy. Grain refinement was obtained under these conditions.

2) Electrochemical corrosion tests including potentiodynamic polarization, linear polarization and electrochemical impedance before and after prolonged immersion of alloy specimens showed that the corrosion resistance of alloy specimens increased in the order: as-cast alloy < mechanically vibrated < ultrasonically vibrated.

3) Surface characterization of corroded specimens substantiated the results of electrochemical tests. Surface of the as-cast alloy specimen suffers from severe corrosion attack compared to the mechanically vibrated and ultrasonically vibrated specimens which show the least corroded surface.

4) EDX analysis before corrosion testing showed that the UV specimen contains the highest content of oxygen indicating a more protective layer. After corrosion testing, the UV specimen contains the least chloride content indicating higher corrosion resistance.

## References

1. Staigera MP, Pietaka AM, Huadmaia J, Dias G., *Biomater.*, 27 (2006) 1728e34.
2. Song GL, Andrej A., *Adv Eng Mater*, 1 (1999) 11e33.
3. Li L, Gao J, Wang Y., *Surf. Coat. Technol.*, 185 (2004) 92e8.
4. Witte F, Kaese V, Switzer H, Meyer-Lindenberg A, Wirth CJ, Windhag H., *Biomater.*, 26 (2005) 3557e63.
5. Witte F, Fischer J, Nellesen J, Crostack H, Kaese V, Pischd A, et al., *Biomater.*, 27 (2006) 1013e8.
6. Heublein B, Rohde R, Kaese V, Niemeyer M, Hartung W, Haverich A, *Heart*, 89 (2003) 651e6.
7. Zartner P, Cesnjevar R, Singer H, Weyand M., *Catheter. Cardiovasc. Interv.*, 66 (2005) 590e4.
8. Schranz D, Zartner P, Michel-Behnke I, Akinturk H., *Catheter. Cardiovasc. Interv.*, 67 (2006) 671e3.
9. Kuwahara H, Al-Abdullat Y, Mazaki N, Tsutsumi S, Aizawa T., *Mater. Trans.*, 42 (2001) 1317e21.
10. Chen Y, Zhang SX, Li JN, Song Y, Zhao CL, Zhang XN. *Mater. Lett.*, 64 (2010) 1996.
11. Bobby KM, Singh RK, *Biomater.*, 29 (2008) 2306.
12. Girgis NN, Ghayad IM, *Advances in Materials Science and Engineering*, Volume 2013, Article ID 532896.
13. Wan Y, Xiong G, Luo H, He F, Huang Y, Zhou X, *Materials and Design*, 29 (10) (2008) 2034.
14. Zhang S, Zhang X, Zhao C, Li J., Song Y, Xie C, Tao H, Zhang Y, He Y, Jiang Y, *Acta Biomater.*, 6 (2) (2010) 626.
15. Nie KB, Wang XJ, Hu XS, Xu L, Wu K, Zheng MY, *Mater. Sci. Eng. A*, 528 (2011) 5278
16. Z. Zhi-qiang, L. Qi-chi, C. Jian-zhong, *Trans. Nonferrous Met. Soc. China*, 18 (2008) s113.
17. Jian XG, Thomas TM, Han QY, *Scr. Mater.*, 54 (5) (2006) 893–896.
18. Abramov V., Abramov O., Bulgakov V., Sommer F., *Mater. Lett.*, 37 (1/2) (1998) 27.
19. Hara N, Kobayahsi Y, Kagaya D, Akao N, *Corros. Sci.*, 39 (1997) 194.
20. H. H. Uhlig, R. W. Revie, *Corrosion and Corrosion Control, an Introduction to Corrosion Science and Engineering*. 3<sup>rd</sup> edd., p.35.
21. Nordlien JH, Ono S, Masuko N, Nisancioclu K, *Corros. Sci.*, 39 (1997) 1397.
22. Zhang S., Zhang X. , Zhao C., Li J., Song Y., Xie C., Tao H., Zhang Y, He Y., Jiang Y., Bian Y., *Acta Biomater.*, 6 (2010) 626.
23. Lei T., Tang W., Cai S.H., *Corros. Sci.*, 54 (2012) 270.